Heliyon 9 (2023) e21725

Contents lists available at ScienceDirect

Heliyon

journal homepage: www.cell.com/heliyon

Analytical and numerical (FEA) solution for steady-state heat transfer in generic FGM cylinder coated with two layers of isotropic material under convective-radiative boundary conditions

Palash Das [a,b], Md. Ashraful Islam [a,*], Dipayan Mondal [a], Md. Sharier Nazim [a,b]

[a] Department of Mechanical Engineering, Khulna University of Engineering & Technology, Khulna, 9203, Bangladesh
[b] Department of Mechanical Engineering, Bangladesh Army University of Science and Technology, Saidpur, Bangladesh

ARTICLE INFO

Keywords:
Functionally graded material (FGM)
Analytical solution
Finite element analysis (FEA)
Three-layer sandwich disks
Thick cylinder
Heat transfer

ABSTRACT

An investigation was carried out in order to develop an accurate analytical solution and a numerical (FEA) solution for steady-state heat transfer in a circular sandwich structure incorporated with convective-radiative boundary conditions. The dimensional governing equations and boundary conditions were developed in the form of a 4th order algebraic equation, and then the solution was obtained using Ferrari's method. By solving for the roots of the quartic equation, we were able to determine the dimensionless temperature fields of the FG sandwich composite. The findings obtained utilizing the exact analytical solution for the FG sandwich composite under thermal loads were satisfactorily validated against those data obtained using the Galerkin finite element approximation. The impact of geometric and thermo-physical characteristics, such as Biot number $(Bi_{i=1,2})$, Inner and outer surface thickness ratio $\left(r_{i=1,2}/R_o\right)$, ambient temperature ratio (θ_d), radiation-conduction parameter (N_r), and thermal conductivity ratio $\left(\lambda_3/\lambda_1\right)$ on the efficiency of heat transfer, has also been studied. This study reveals the distinct effect of Biot number on the inner and outer layers of the composite cylinder. It shows that Bi_1 has a negligent effect on temperature distribution; on the other hand, the outer surface ($Bi_2 \leq 1$) minimizes temperature variation. However, for design consideration, a thicker inner face sheet is not recommended in high thermal load, as $N_r > 4$ has an insignificant impact on inner surface thickness on top surface temperature. Moreover, the outer surface temperature appears to be more sensitive to θ_d than the radiation-convection side. Furthermore, the given analytical solution is adequately verified against the proposed FEA method, having an error of less than 1.5 %.

1. Introduction

The functionally graded materials (FGMs) are composites having two or more phases and constantly varying compositions along spatial positions. FGMs have recently attracted the interest of numerous experts because they are anticipated to be highly heat-resistant materials under situations of high temperature or temperature gradient. So the study of heat transfer plays a pivotal role in the practical implementation of FGMs in extremely high-temperature environments.

* Corresponding author.
E-mail address: md.islam@me.kuet.ac.bd (Md.A. Islam).

https://doi.org/10.1016/j.heliyon.2023.e21725
Received 11 May 2023; Received in revised form 18 September 2023; Accepted 26 October 2023
Available online 28 October 2023

A significant amount of effort has been put in by a variety of researchers to comprehend the heat transfer characteristic of FGMs. Using the boundary integral approximation and the Gelerekin approximation in the finite element analysis (FEA), 3D and 2D rotating and non-rotating FGM structures subjected to heat transfer were solved for exponentially varying characteristics [1]. The 2-D heat conduction problems are frequently solved using the boundary element method (BEM), which uses triple reciprocity relations [2]. Guo et al. [3,4] examined the thermally shocked behavior of fractured FGMs structures. Under convective boundary conditions, two-dimensional anisotropic FGM Cauchy problems have been studied [5]. An exact analytical solution for the transient heat conduction in an annular cylinder of an FGM was given by Babaei et al. [6]. Zenkour [7] describes the thermomechanical behavior of an FG sandwich structure with traction under Dirichlet thermal boundary conditions (B.Cs). A lot of research has been done on a non-Fourier heat transfer analysis for moving and constant heat flux with convective-radiative B.Cs for cylinders and spheres [8–12]. Besides heat transfer, a lot of research has been carried out in the context of FGM structure. A. Tounsi et al. study the vibratory, buckling, and bending characteristics of a FGM porous beam using the first-order shear deformation theory. They demonstrate that the influence of material distribution, geometrical configuration, boundary conditions, and porosity distributions has a significant effect on critical buckling and natural frequencies on FGM structures [13–16]. Additionally, the impact of imperfection sensitivity on vibration response in 2D-FGPs was also investigated [17]. Moreover, as part of the enhancement of the computational model of the FG structure, the element stiffness matrix for FG nanoplates was evaluated in a unique way using the boundary element method [18]. Aside from elastic materials, substantial research has been conducted on free vibration on various viscoelastic material models on FGM [19–21]. In addition to the linear shear deformation theory, the sinusoidal shear deformation model has been used to explore the combined effects of porosity and elastic parameters on sandwich structures [22].

A large number of analytical and numerical solutions are carried out when the FGM structures are subjected to mechanical load in the elastic zone under various material inhomogeneities [23–29]. According to a power law in the material properties, Bayat et al. [30] analyze the displacements and stress fields of FGM spheres under thermomechanical loadings. Other scholars, however, have done comparable work for axisymmetry structures having rotational or irrotational considerations with constant poisson ratio and varying material inhomogeneities index [31–42]. Moreover, both steady and unsteady asymmetric thermomechanical-loaded cylinders have been examined [43–45]. N. Djilali et al. reported an HSDT-based investigation of nonlinear cylindrical bending of FG plates reinforced by single-walled carbon nanotubes in an elevated temperature environment [46]. A similar but dynamic analysis has been done on FG carbon nano tube [47]. Apart from elastic analysis, a significant amount of work is being done on elastoplastic analysis of FGM structures [48,49]. The stress and displacement fields of FGM are studied by NEMATOLLAHI et al. [50], who investigate the influence of a magnetic field in addition to thermo-mechanical loads on rotating FGM spheres. Arefi et al. [51] given a nonlinear electro-thermo-mechanical model of a thick spherical vessel made of functional dependent piezoelectric materials.

Cylindrical Sandwiches,conversely, a multilayer structures are mostly characterized by their prevalence because of their excellent strength-to-weight ratio, heat resistant capacity, and extensive use in a variety of technological applications such as nuclear reactor and aircraft [52]. To solve the problem of how heat conduction takes place through a multilayer structure, a number of analytical and numerical methods have been suggested. PS Reddy et al. proposed an analytical solution for heat and mass transmission in a thermomagnetic environment for a nanofluid. They investigated the impact of convective boundary conditions along with thermal radiation on flow of nanofluid in saturated porous media [53–56]. Additionally, heat transfer and flow analysis of a water- Maxwell nanofluid between two rotating disks under convective boundary condition are numerically investigated [57]. Delouei et al. [58] came up with an exact mathematical solution for the heat conduction equation in spherical coordinates of FGM with material properties that change in both radial (r) and tangential (θ) directions. For analyzing the variation of characteristics, the power law is used. The temperature profiles for different asymmetric boundary conditions have been generated for FG cylindrical segments exposed to general boundary conditions [59]. Besides, the problem of axial heat flow in an axisymmetric cylinder (r,z) is solved using Fourier transform [60]. The conductivity parameter in this scenario is taken to be a function of radial and tangential coordinates that follows a power law. Moreover, the method of variable separation is utilized to solve the heat equation in polar coordinates in order to have a thorough grasp of the thermal behavior of FGM structures [61]. Kayhani et al. [62] propose a stable analytical solution for heat conduction in a cylindrical multilayer composite laminate with varying fiber orientation between layers. Manthena et al. [63] give an unsteady analysis of FG cylinder heat conduction under temperature-dependent thermal conductivity. Laplace transform, a semi-analytical approach, and numerical inverse Laplace transform employing Meromorphic function were used to solve 2-D transient heat conduction of laminated spherical structure [64]. The non-transient heat conduction problem encountered in non-isotropic multilayered media with Dirichlet B.C.s was described by Ma et al. [65] using an analytical solution. Furthermore, in a study conducted by Kumar et al. [66], the Finite Difference Method (FDM) was employed to address the solution of a one-dimensional heat conduction equation within a multilayer Thermal Protection System (TPS) that featured a radiative boundary condition. Torabi et al. [67] investigated the temperature distribution in dual layer composite walls under the influence of convection and radiation boundary conditions. To analyze this phenomenon, they employed the differential transform (DT) method. Wang et al. [68] used Ferrari's methodology to conduct a complete thermal study in a rectangular FG sandwich covered with isotropic materials in radiative-convective conditions.

Moreover, A. A. Bousahla et al. [69] investigated thermal stability under varying thermal expansion coefficients.

However, in most earlier studies, the inhomogeneity of materials was thought to be either power law or exponential law. To the best of the author's knowledge, there are no known analytical or numerical (FEA) solutions for cylindrical composite structures operating in radiation-convection environments. In addition, the heat transfer behavior of FG circular sandwich structures under the above-mentioned environment is not well understood. Furthermore, there is little to no work in the literature that addresses thermal conductivity in the generalized formula that does not use singly power law and exponential law. The vast majority of works done in the past are solely concerned with a constant temperature and convection boundary condition, rather than a combination of convection and radiation since radiation is unavoidable. For instance, developing thermal coatings and shielding are examples of such cases. The

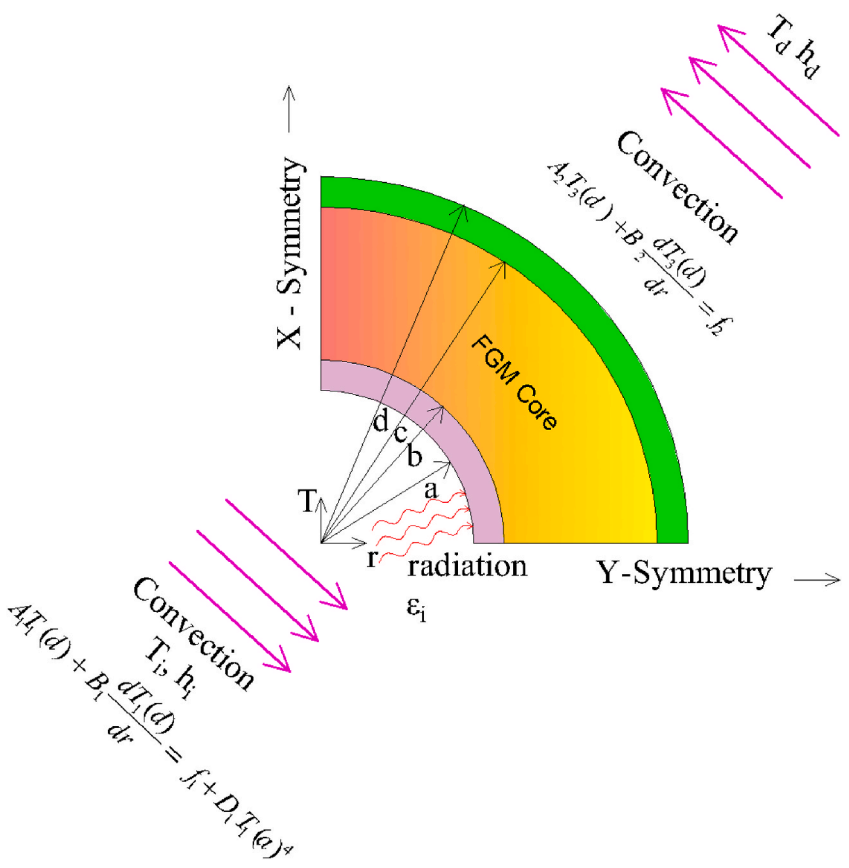

Fig. 1. Configuration of FGM composite cylinder.

goal of this paper is to develop a one-dimensional analytical and numerical model, for the first time to study the convective-radiative heat transfer behavior of a FG sandwich cylinder under generalized material parameters. The thermally loaded vessel was also modeled using finite element analysis (FEA), where a FE code (USDFLD) was used to represent the continuous variation of thermal conductivity along with the vessel's thickness. Afterward, we compared the exact and FE findings. The findings will emphasize the influence of the Biot number, the radiation-conduction parameter, the ratio of the temperature of the inner layer to that of the outermost layer, and the thickness of coated materials on temperature distribution in FG sandwich cylinders.

2. Problem formulation

In this study, a multilayered composite cylinder with isotropic coatings and a generalized FGMs core are considered (Fig. 1) where a, b, c and d are inner, intermediates, and outer radial dimensions. Thermal conductivities of inner coating and outer coating k_1 and k_3, respectively. According to the literature [70] a generic function of thermal conductivity along the thickness direction is considered for FGM core has been shown in Eq. (1) as follows

$$k(r) = \begin{cases} k_1 & \text{in inner coating } (\mathrm{r} \in [\mathrm{a}, \mathrm{b}]) \\ k_1 \left(\frac{r}{b}\right)^m e^{\gamma \left\{ \left(\frac{r}{b}\right)^s - 1 \right\}} & \text{in FGMs core } (\mathrm{r} \in [\mathrm{b}, \mathrm{c}]) \\ k_3 & \text{in inner coating } (\mathrm{r} \in [\mathrm{c}, \mathrm{d}]) \end{cases} \tag{1}$$

where m and s are the material's inhomogeneity constants. The additional constants γ, k_3 are given by

$$\gamma = \frac{m \ln\left(\frac{b}{c}\right) + \ln\left(\frac{k_3}{k_1}\right)}{b^s \left(c^s - b^s\right)}, k_3 = k_1 \left(\frac{c}{b}\right)^m e^{\gamma \left\{ \left(\frac{c}{b}\right)^s - 1 \right\}}$$

Heat conduction in a FG composite cylinder with an external surface subject to convection and an internal surface subject to coupled convection-radiative heat transfer is considered in this simplified model (see Fig. 1). Moreover, no volumetric heat is anticipated to be produced. The temperature distribution for composite cylinder are governed by the following equations (Eq. (2)):

$$\begin{aligned}
&\frac{d}{dr}\left[rk_1\frac{dT_1}{dr}\right]=0 \quad a<r<b\\
&\frac{d}{dr}\left[rk(r)\frac{dT_2}{dr}\right]=\frac{d}{dr}\left[rk_1\left(\frac{r}{b}\right)^m e^{\gamma\left\{\left(\frac{r}{b}\right)^s-1\right\}}\frac{dT_2}{dr}\right]=0 \quad b<r<c\\
&\frac{d}{dr}\left[rk_2\frac{dT_3}{dr}\right]=0 \quad c<r<d
\end{aligned} \tag{2}$$

As the cylinder is subjected to a high thermal load, radiation heat transfer predominated in addition to convection. For brevity, it is considered the outer surface subject to convection only. A general linear (convection) and non-linear (convection-radiation) B.C. can be written as follows (Eq. (3)):

$$A_1T_1(a)+B_1\frac{dT_1(a)}{dr}=f_1+D_1T_1(a)^4, A_2T_3(d)+B_2\frac{dT_3(d)}{dr}=f_2 \tag{3}$$

where $A_{i=1,2}, B_{i=1,2}$ are known thermal parameters related to convection and conduction co-efficient. $f_{i=1,2}$ is radiation-convection known parameters and D_1 is the emissivity of the surface in Eq. (3).

Assuming a perfect thermal contact at the interfaces between the coating and FGM core, in order to determine integration constant along with boundary condition additional relation at contact surface can be written as in Eq. (4):

$$\begin{aligned}
&T_1|_{r=b}=T_2|_{r=b}\\
&T_2|_{r=c}=T_3|_{r=c}-k_1\frac{dT_1}{dr}\bigg|_{r=b}=-k_1\left(\frac{r}{b}\right)^m e^{\gamma\left\{\left(\frac{r}{b}\right)^s-1\right\}}\frac{dT_2}{dr}\bigg|_{r=b}-k_1\left(\frac{r}{b}\right)^m e^{\gamma\left\{\left(\frac{r}{b}\right)^s-1\right\}}\frac{dT_2}{dr}\bigg|_{r=c}=-k_3\frac{dT_3}{dr}\bigg|_{r=c}
\end{aligned} \tag{4}$$

2.1. Solution utilizing Ferrari's technique

The generalized exat analytical solutions for Eq. (2 a, b, c) can be expressed as follows in Eq. (5):

$$\begin{aligned}
&T_1(r)=\xi_1\ln(r)+\xi_2\\
&T_2(r)=\int\left(\frac{\xi_3}{\left(\frac{r}{b}\right)^{m+1}e^{\gamma\left\{\left(\frac{r}{b}\right)^s-1\right\}}}\right)dr+\xi_4\\
&T_3(r)=\xi_5\ln(r)+\xi_6
\end{aligned} \tag{5}$$

Eq. (5 b) can be simplified as:

$$T_2(r)=\xi_3\psi(r)+\xi_4 \tag{6}$$

where; $\psi(r)=\int\left(\frac{dr}{\left(\frac{r}{b}\right)^{m+1}e^{\gamma\left\{\left(\frac{r}{b}\right)^s-1\right\}}}\right)$.

The above integration (Eq. (6)) can be expressed in terms of the Whittaker function [71].

Where, $\xi_1, \xi_2, \xi_3, \xi_4, \xi_5, \xi_6$ are integration constants.

Substituting Eqs. (5a), (5b) and (6) into Eqs. (3) and (4), the following equations can be obtained (Eq. (7))

$$\begin{aligned}
&\xi_1\left(A_1\ln(a)+\frac{B_1}{a}\right)+A_1\xi_2=f_1+D_1(\xi_1\ln(a)+\xi_2)^4\\
&A_2\xi_6+\left(A_2\ln(d)+\frac{B_2}{d}\right)\xi_5=f_2\\
&\xi_1\ln(b)+\xi_2=\xi_3\psi(b)+\xi_4\\
&\frac{\xi_1}{b}=\xi_3\frac{d\psi(r)}{dr}\bigg|_{r=b}\\
&\xi_3\psi(c)+\xi_4=\xi_5\ln(c)+\xi_6\\
&\xi_3\frac{d\psi(r)}{dr}\bigg|_{r=c}=\xi_5/c
\end{aligned} \tag{7}$$

The above equation (7)(c)-7(f) can be rearranged as follows:

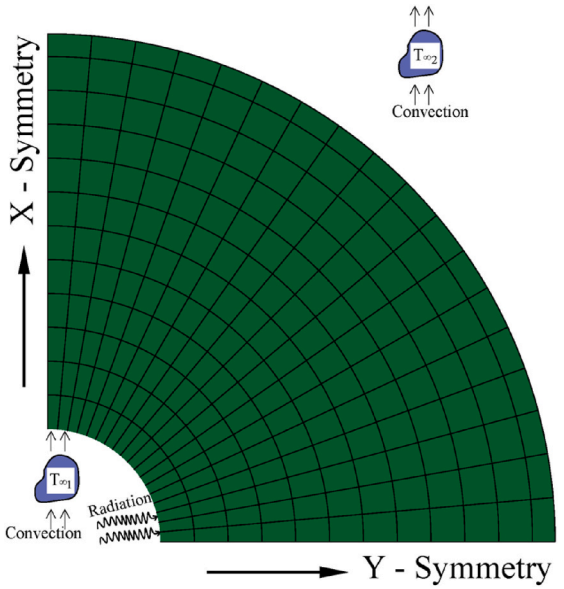

Fig. 2. Meshing with Boundary Conditions (B.C.s) of the numerical model.

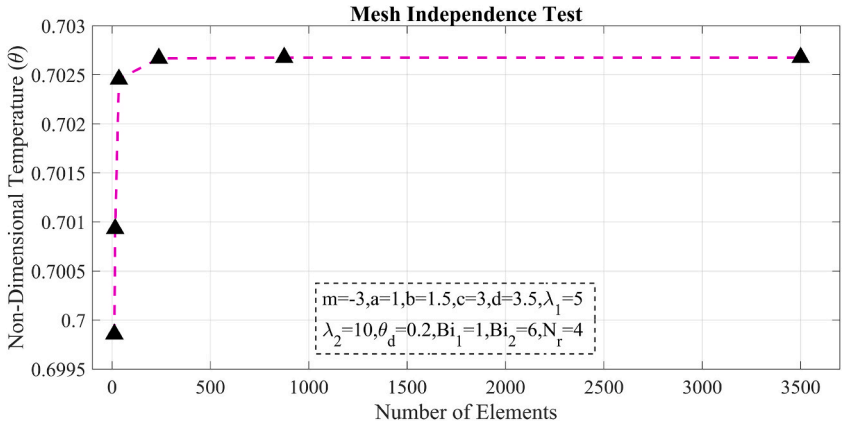

Fig. 3. Grid independence test of the problems.

$$\xi_3 = p\xi_1$$
$$\xi_4 = q\xi_1 + \xi_2$$
$$\xi_5 = w\xi_1$$
$$\xi_6 = g\xi_1 + \xi_2 \tag{8}$$

Where; $p = \dfrac{1}{b\left.\dfrac{d\psi(r)}{dr}\right|_{r=b}}, q = \ln(b) - \dfrac{\psi(r)}{b\left.\dfrac{d\psi(r)}{dr}\right|_{r=b}}, w = \dfrac{c}{b}\dfrac{\left.\dfrac{d\psi(r)}{dr}\right|_{r=c}}{\left.\dfrac{d\psi(r)}{dr}\right|_{r=b}}$

$$g = p\psi(c) + q - \ln(c)w$$

Substituting Eq. (8)(c)-8(d) into Eq. (7b), the expression for ξ_2 is given by

$$\xi_2 = u - v\xi_1 \tag{9}$$

Where

$$u = \frac{f_2}{A_2}, v = g + \ln(d)w + \frac{B_2 w}{dA_2}$$

Table 1
A comparison of analytical (Eq. (5) a, b, c) and FEM numerical data in the normalized radial direction for different thermal conductivity indices ($m = -3, -4, -5$) at $Bi_2 = 10$.

$\left(\frac{r-a}{d-a}\right)$	Type	$m = -3$		$m = -4$		$m = -5$	
		θ_1		θ_1		θ_1	
		Value	%Err.	Value	%Err.	Value	%Err.
0	Anal.	0.901	0.00	0.923	0.00	0.943	0.21
	FEM	0.901		0.923		0.945	
0.1	Anal.	0.801	0.12	0.843	0.11	0.883	0.23
	FEM	0.802		0.844		0.885	
0.2	Anal.	0.720	0.41	0.778	0.13	0.834	0.35
	FEM	0.723		0.779		0.837	
0.4	Anal.	0.555	0.54	0.624	0.16	0.698	0.42
	FEM	0.558		0.625		0.701	
0.5	Anal.	0.455	0.43	0.529	0.37	0.599	0.50
	FEM	0.457		0.531		0.602	
0.8	Anal.	0.314	0.31	0.314	0.63	0.331	0.61
	FEM	0.315		0.316		0.333	
1	Anal.	0.280	0.35	0.264	0.70	0.248	0.80
	FEM	0.281		0.266		0.250	

Table 2
A comparison of the analytical data (Eq. (5) a, b, and c) with the numerical data from the FEM in the normalized radial direction for several parameters at $m = -3$.

$\left(\frac{r-a}{d-a}\right)$	Type	$N_r = 4$		$\theta_d = 0.8$		$\lambda_3/\lambda_1 = 15$	
		θ_1		θ_1		θ_1	
		Value	%Err.	Value	%Err.	Value	%Err.
0	Anal.	0.908	0.22	0.979	0.30	0.964	0.31
	FEM	0.910		0.982		0.968	
0.1	Anal.	0.814	0.36	0.955	0.31	0.766	0.39
	FEM	0.817		0.958		0.769	
0.2	Anal.	0.738	0.40	0.936	0.42	0.604	0.82
	FEM	0.741		0.940		0.609	
0.4	Anal.	0.583	0.68	0.897	0.44	0.390	0.79
	FEM	0.587		0.901		0.393	
0.5	Anal.	0.504	0.99	0.877	0.45	0.329	0.91
	FEM	0.509		0.881		0.332	
0.8	Anal.	0.357	0.84	0.840	0.35	0.261	1.53
	FEM	0.360		0.843		0.265	
1	Anal.	0.325	0.92	0.832	0.37	0.253	1.58
	FEM	0.328		0.835		0.257	

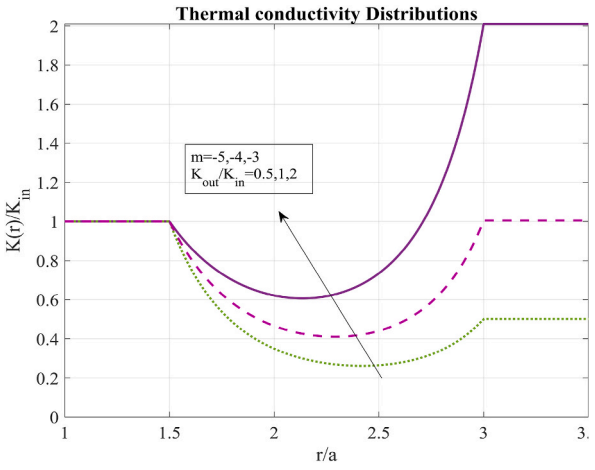

Fig. 4. Generalized distributions of thermal conductivity.

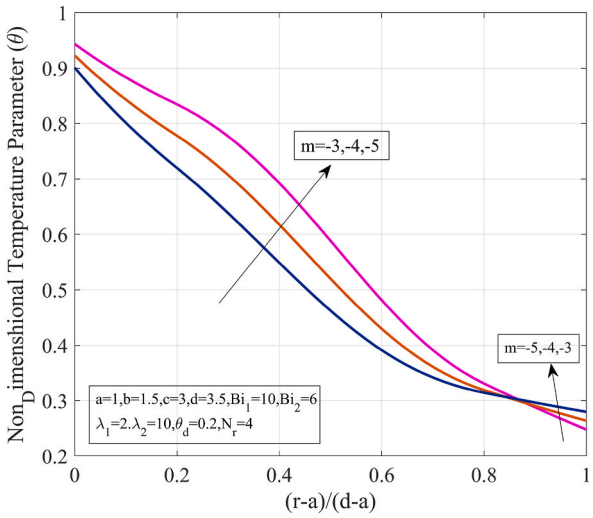

Fig. 5. Effect of the generalized materials inhomogeneity parameter on the dimensionless temperature.

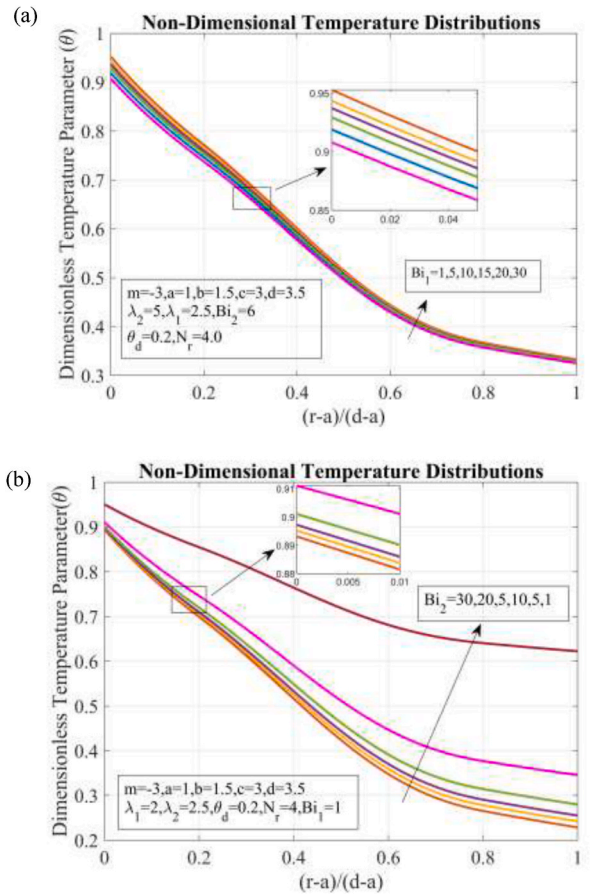

Fig. 6. Effect of the generalized materials inhomogeneity parameter ($m = -3$) on the dimensionless temperature for various values of (a) the inner surface Biot number (Bi_1) and (b) the outer surface Biot number (Bi_2).

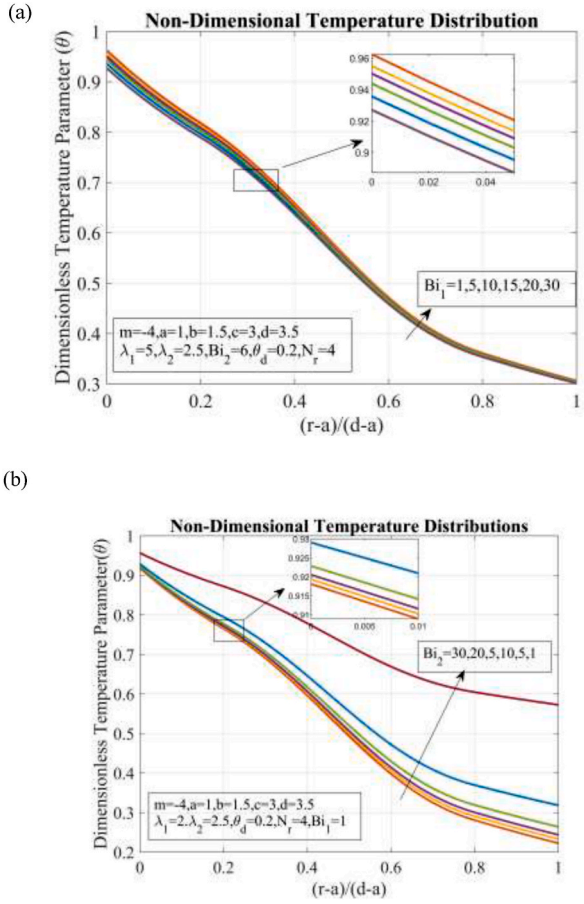

Fig. 7. Effect of the generalized materials inhomogeneity parameter ($m = -4$) on the dimensionless temperature for various values of (a) the inner surface Biot number (Bi_1) and (b) the outer surface Biot number (Bi_2).

again, substituting Eq. (9) into (7a) will be resulted in:

$$\xi_1\varphi_1 = \varphi_2 + D_1(\xi_1\tau + u)^4$$

Where;

$$\varphi_1 = A_1 \ln(a) + \frac{B_1}{a} - A_1 v \tag{10}$$

$$\varphi_2 = f_2 - A_1 u$$

$$\tau = \ln(a) - v$$

Eq. (10) can be rewritten as:

$$x_1 {C_1}^4 + x_2 {C_1}^3 + x_3 {C_1}^2 + x_4 C_1 + x_5 = 0 \tag{11}$$

where

$$x_1 = D_1\tau^4, x_2 = 4uD_1\tau^3, x_3 = 6u^2D_1\tau^2, x_4 = 4u^3D_1\tau - \varphi_1, x_5 = u^4D_1 + \varphi_2$$

The solution of Eq. (11) can be obtained using the well-known Ferrari's method [72]. After the substitution $C_1 = y - \frac{x_2}{4x_1}$ Eq. (11) become [71]

$$y^4 + \delta_1 y^2 + \delta_2 y + \delta_3 = 0 \tag{12}$$

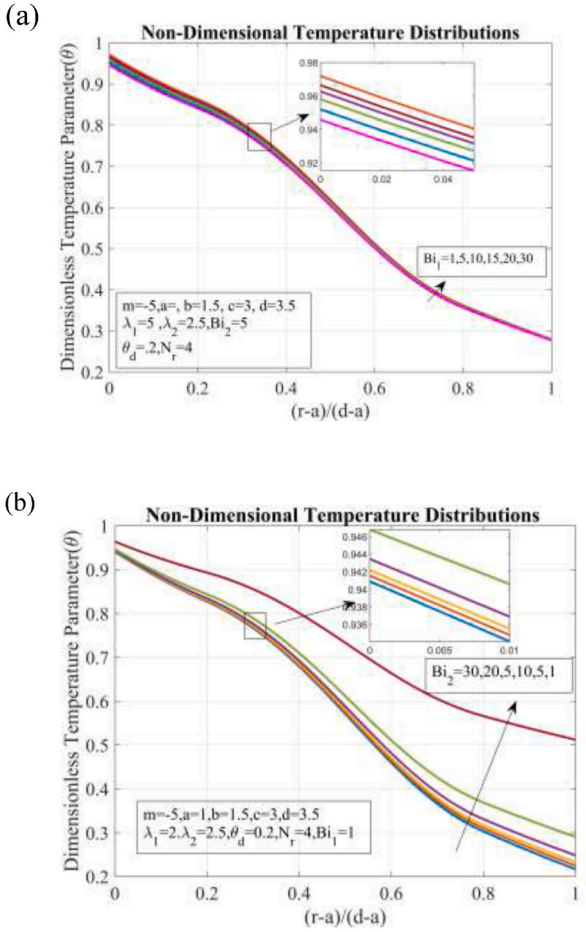

Fig. 8. Effect of the generalized materials inhomogeneity parameter ($m = -5$) on the dimensionless temperature for various values of (a) the inner surface Biot number (Bi_1) and (b) the outer surface Biot number (Bi_2).

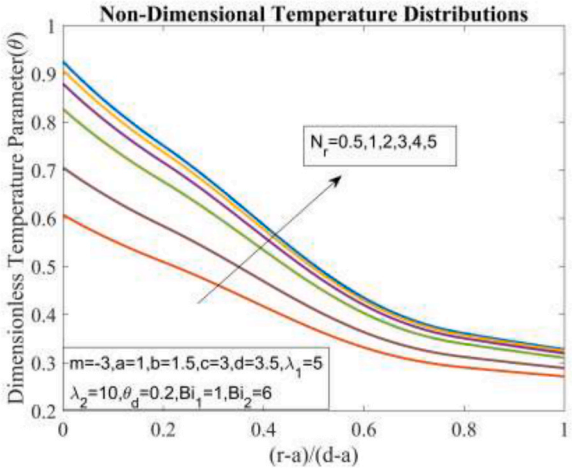

Fig. 9. The influence of the radiation-conduction parameter (N_r) on the dimensionless temperature fields of a circular FG sandwich structure along non-dimensional radius.

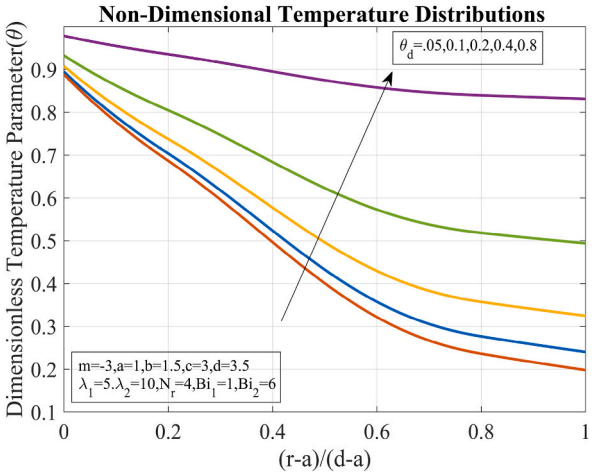

Fig. 10. The influence of the ambient temperature ratio (θ_d) on the dimensionless temperature field of a circular FG sandwich structure along non-dimensional radius.

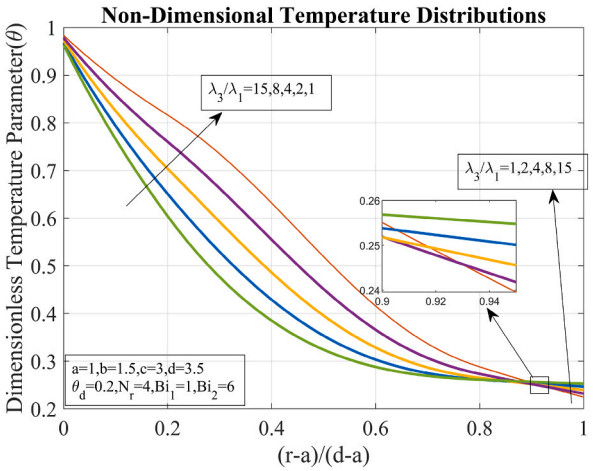

Fig. 11. Effect of the conductivity ratio $\left(\lambda_3/\lambda_1\right)$ on the non-dimensional temperature fields of FG circular sandwich structure.

Where,

$$\delta_1 = \frac{x_3}{x_1} - \frac{3{x_2}^2}{8{x_1}^2}$$

$$\delta_2 = \frac{x_4}{x_1} - \frac{x_2 x_3}{2{x_1}^2} + \frac{{x_2}^3}{8{x_1}^3}$$

$$\delta_3 = \frac{x_5}{x_1} - \frac{x_2 x_4}{4{x_1}^2} + \frac{{x_2}^2 x_3}{16{x_1}^3} - \frac{3{x_2}^4}{256{x_1}^4}$$

Introducing new parameter s, which satisfy the following equation [71].

$$8s^3 - 4\delta_1 s^2 - 8\delta_3 s + \left(4\,\delta_1\delta_3 - {\delta_2}^2\right) = 0$$

then Eq. (12) can be written as:

$$\left(y^2 + s + \sqrt{2s - \delta_1}\, y - \frac{\delta_2}{2\sqrt{2s - \delta_1}}\right)\left(y^2 + s - \sqrt{2s - \delta_1}\, y + \frac{\delta_2}{2\sqrt{2s - \delta_1}}\right) = 0$$

The given equation has four roots, two of the roots in the above equation are imaginary, whereas the other two are real. One of them of two real roots is positive, while the other is negative. Considering the positive one then it can be expressed as:

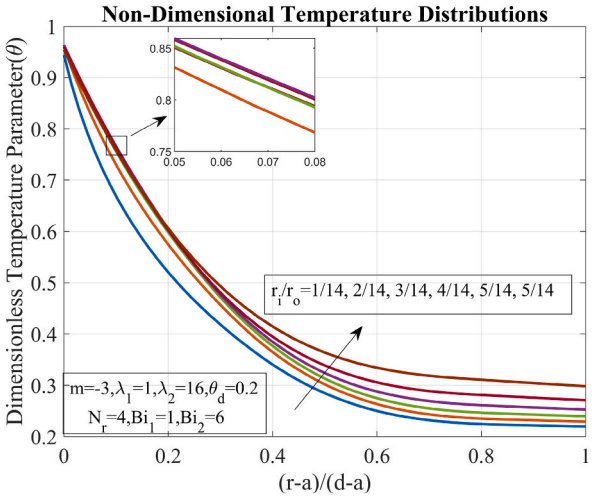

Fig. 12. The influence of the thickness ratio of the inner surface coating on the non-dimensional temperature distribution.

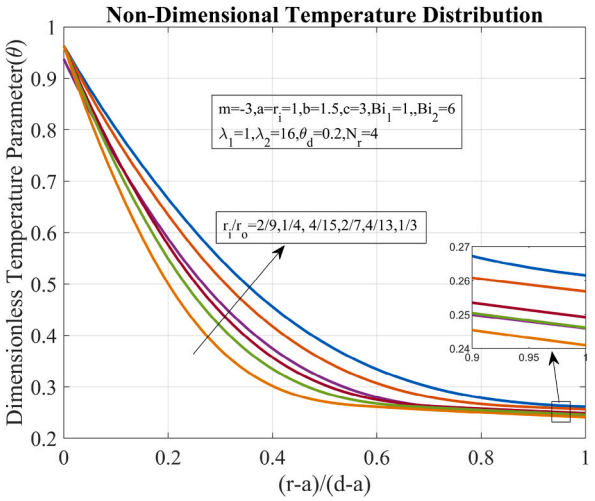

Fig. 13. The effect of the thickness of the outer surface coating on the non-dimensional temperature distribution.

$$y = -\frac{1}{2}\sqrt{2s-\delta_1} + \frac{1}{2}\sqrt{-2s-\delta_1+\frac{2\delta_2}{\sqrt{2s-\delta_1}}}$$

From above equation ξ_1 can be expressed as:

$$\xi_1 = -\frac{1}{2}\sqrt{2s-\delta_1} + \frac{1}{2}\sqrt{-2s-\delta_1+\frac{2\delta_2}{\sqrt{2s-\delta_1}}} - \frac{x_2}{4x_1} \tag{13}$$

Substituting Eq. (12) into Eqs. (8) and (9), the general integration constant $\xi_2, \xi_3, \xi_4, \xi_5, \xi_6$ can be obtained. After that, the FG composite cylinder's temperature field may be calculated.

2.2. Finite element analysis (FEA)

In this problem, a standard Galerkin discretization approach of finite element method is used to solve the differential equation (12 a, b, c). In this discretization the size of each element is equal and total domain is divided into N elements and then equation is converted into simultaneous equations.

$$\sum_{j=1}^{2} K_{ij} T_j^e = L_i^e \quad ; i = 1,2 \quad e = 1,2,.....N$$

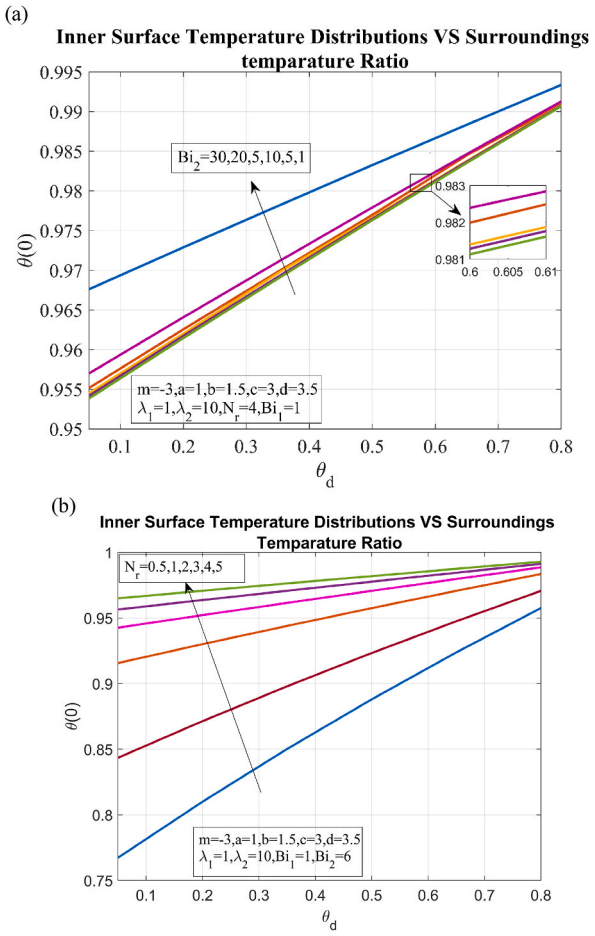

Fig. 14. The influence of the ambient temperature ratio (θ_d) on the inner surface temperature of the FG sandwich cylinder with various values of (a) Biot number (Bi_2) and (b) radiation-conduction parameter (N_r).

$$\begin{cases} K_{ij}^e = \int_{r_e}^{r_{e+1}} k_m r \frac{d\Omega_i^e}{dr}\frac{d\Omega_j^e}{dr}dr + \left[k_m r \Omega_i^e \frac{d\Omega_j^e}{dr}\right]_{r_e}^{r_{e+1}} \quad Where, m = 1,3 \quad r \in [a,b] \cup [c,d] \\ K_{ij}^e = \int_{r_e}^{r_{e+1}} \left[bk_1\left(\frac{r}{b}\right)^{m+1} e^{\gamma\left\{\left(\frac{r}{b}\right)^s - 1\right\}}\right]\frac{d\Omega_i^e}{dr}\frac{d\Omega_j^e}{dr}dr + \left[bk_1\left(\frac{r}{b}\right)^{m+1} e^{\gamma\left\{\left(\frac{r}{b}\right)^s - 1\right\}}\Omega_i^e\frac{d\Omega_j^e}{dr}\right]_{r_e}^{r_{e+1}} \quad r \in [b,c] \\ L_i^e = 0 \end{cases}$$

Where Ω_i^e is linear interpolation function T_j^e unknown nodal temperature. The aforementioned mathematical FE model of heat transfer in cylindrical co-ordinate was implemented using the commercial FEA code, ABAQUS. One-quarter of the geometry has been addressed in the FEA model due to the axisymmetric nature of the boundary condition and geometry. The system is discretized using an 8-node quadratic heat transfer quadrilateral (DC2D8) element. Fig. 2 shown the meshing of the system with B.C.s. The final FEM model was constructed using 3500 elements that were optimized via grid independent test (Fig. 3). A FORTRAN code USDFLD was developed and then coupled with ABAQUS to capture nonlinear material property variations along the radius.

3. Result and discussion

In this preceding section, several non-dimensional characteristics were incorporated to enable more comprehensive studies and to make the problem as generalized as feasible.

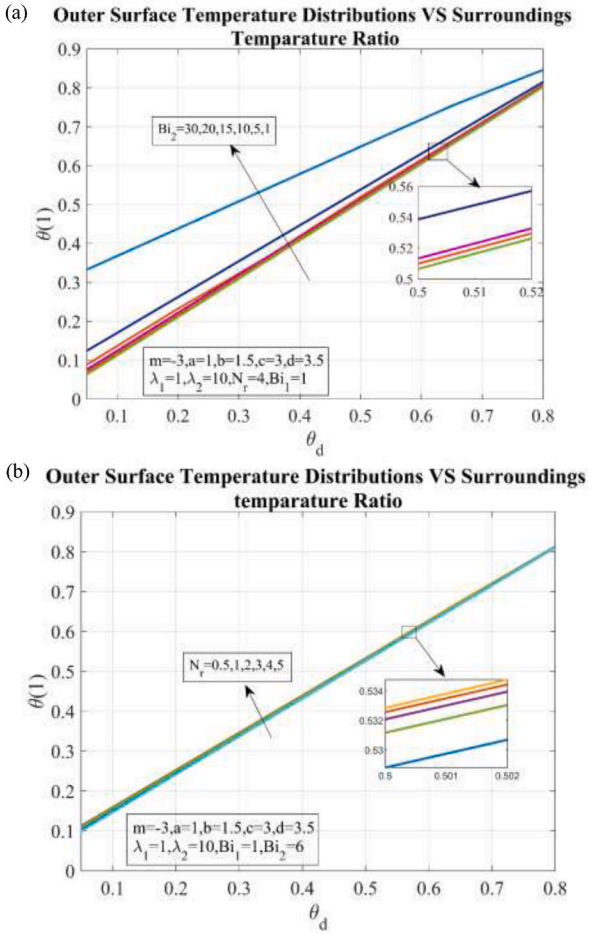

Fig. 15. The influence of the ambient temperature ratio (θ_d) on the outer surface temperature of the FG sandwich cylindrical structure with various values of (a) Biot number (Bi_2) and (b) radiation-conduction parameter (N_r).

$$\theta_j = T_j/T_i \ (j = 1,2,3), \theta_d = T_d/T_i, R = \frac{r-a}{d-a}, \frac{r_j}{R_o}(j = 1,2)$$

$$\lambda_j = k_j/k_{ref} \ (j = 1,3), Bi_j = h_j L/k_{ref} \ (j = 1,2), N_r = \frac{\sigma \varepsilon_1 L T_u^{\ 3}}{k_{ref}} \ \text{Where}, L = \frac{r_o - r_i}{2}$$

3.1. The validation of the results

Since there is presently no solution available for FG circular sandwich cylinders under thermal load (convection-radiation), a number of case studies comparing and contrasting analytical and numerical techniques for investigating temperature distribution across a range of parameters have been provided. (Table-1 and Table −2). Tables 1 and 2 make it abundantly evident that numerical and analytical findings converge where there is an error of less than 1.5 %. This implies that the proposed analytical mathematical model and numerical (FEA) model are robust enough to illustrate the utility and usefulness of this research under all situations.

3.2. Different parameters' effects on temperature distribution

Analytical and numerical solution described in the preceding section for composite FG cylinders with dimensions of $d = 3.5\ a, c = 3\ a, b = 1.5\ a$ and $k_{ref} = 20\ w\ m^{-1}k^{-1}$ are examined. In Fig. 4, a two-layer, isotropic coating on a FGM cylinder that follows a generalized thermal conductivity distribution is shown non-dimensionally. The distribution function is designed to handle a broad variety of laws such as power law, exponential law, or a mix of both. In order to make the analysis more straightforward, the numerical values of the constants in E.q (2) have been modified in this manner in order to generate a condition. In order to replicate the above situation, the constant may be altered in a number of different ways. According to Ref. [70], the numerical values of the constants are as follows: $\gamma = 0.172, s = 4.1$.Then the study was conducted for different values of the inhomogeneity parameter (m), Biot number $(Bi_{i=[1,2]})$,

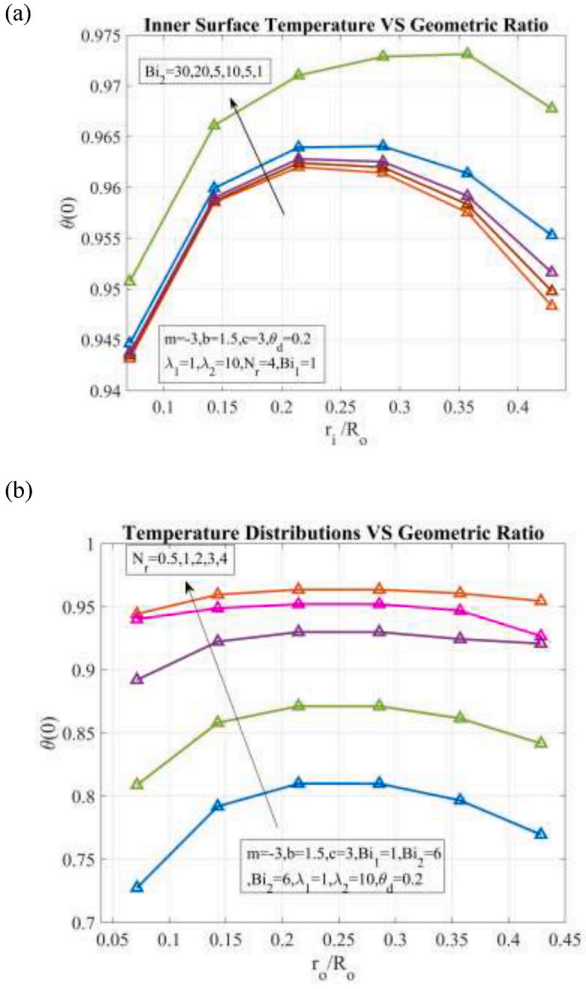

Fig. 16. Influence of inner surface thickness on the inner surface temperature of the FG sandwich with various values of (a) Biot number (Bi_2) and (b) radiation-conduction parameter (N_r).

radiation-conduction parameter (N_r), environment's temperature ratio (θ_d), inner and outer coating thickness $\left(r_{i=1,2}/R_o\right)$, and thermal conductivity ratio $\left(\lambda_3/\lambda_1\right)$.Figs. 5–19 show the numerical findings for the several geometrical and physical factors that influence how the sandwich system behaves in terms of heat flow.

The non-dimensional temperature distribution for different values of material inhomogeneity (m) is displayed in Fig. 5. From the graph, it is evident that temperature rises as m rises between $0 \leq \left(\frac{r-a}{d-a}\right) \leq\sim 0.9$ and temperature decreases as m increases for $0.9 \sim \leq \left(\frac{r-a}{d-a}\right) \leq 1.0$. The cause may be found in the non-uniformity in spatial thermal conductivity variations seen in Fig. 4.

Moreover, the temperature fields in the FG sandwich cylinders are depicted in Fig. 6 a, where the top surface Biot number (Bi_1) is varied while all other parameters remain constant and their values are specified in the figure caption. As shown in Fig. 6 a for a particular value of the inhomogeneity parameter $(m = -3)$, raising the inner surface Biot number marginally raises the temperature of the FG circular composite. This is because the heat transfer rate increases faster when the Biot number goes up, which strengthens the heating impact. Fig. 6 b shows how the temperature changes in the FG composite when the Biot number (Bi_2) of the bottom surface is changed. As demonstrated in Fig. 6 b, the developed temperature of the FG sandwich structure falls as (Bi_2) increases. This is because the more (Bi_2) there is on the surface, the stronger the convection will be. Therefore, more heat will be lost, which will cause the temperature to drop a lot. Additionally, the temperature decrease is smaller from Bi = 5 to 30 and increases dramatically $Bi_2 \leq 1$. Likewise, the explanation of the temperature distributions and patterns for Figs. 5 and 6 are identical to those described earlier in Fig. 6.

In Fig. 9 demonstrate non-dimensional temperature distributions along radial coordinate for different values of radiation-conduction parameter N_r. Each curve in Fig. 9 illustrates that when non-dimensional radius grows, the temperature of the sandwich structure falls. The graph reveals that when the radiation-conduction parameter increases, the temperature of the structure increases at a given radial position. The reason behind is that as N_r increases, radiation heating becomes large enough to raise the

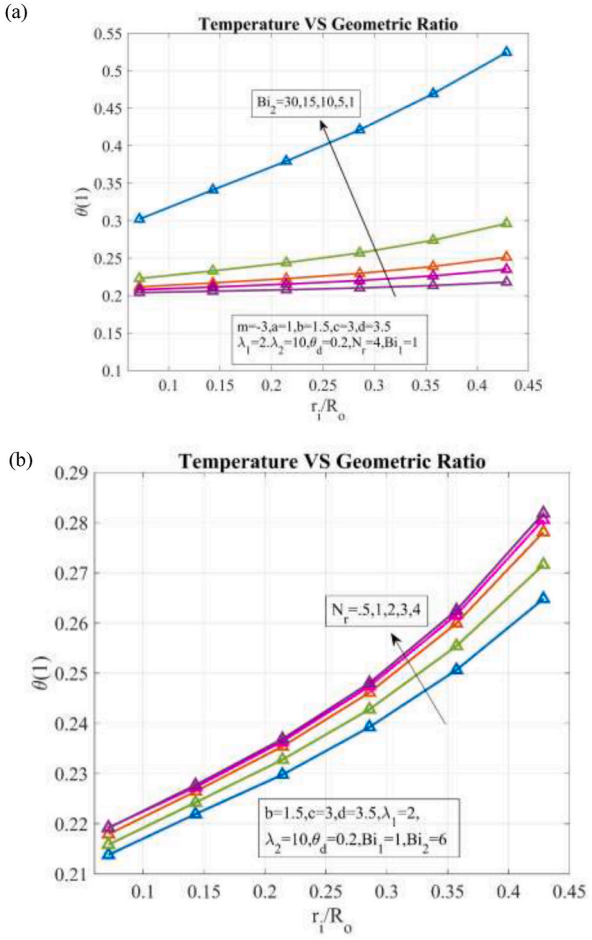

Fig. 17. Influence of inner surface thickness on the outer surface temperature of the FG sandwich with various values of (a) Biot number (Bi_2) and (b) radiation-conduction parameter (N_r).

temperature of the FG sandwich.

The impact of the ambient temperature ratio θ_d concerning temperature distribution on FG sandwiches is shown in Fig. 10. The figure clearly shows that when the temperature ratio grows, radiation predominates and convection weakens, resulting in temperature increases for the particular radial location. The visualization clearly shows that the rate of temperature increase quickens from $\theta_d = 0.05$ to 0.8. Therefore, it is obvious that the outer surface has shown more sensitivity to temperature ratio than the inner surface. Likewise, the temperature difference between the inner and outer surfaces becomes lower as radiation becomes more prevalent and convective heat loss is smaller. In addition, the decreasing nature of temperature along the radius is monotonic up to $\theta_d = 0.05$ to 0.4 after that, higher the ambient temperature ratio $\theta_d \geq 0.8$ flatten the temperature distributions.

In Fig. 11, a dimensionless temperature parameter is displayed in the radial direction for different values of the conduction ratio λ_3/λ_1. The higher the conductance ratio smaller will be the overall thermal resistance results in a lower temperature on the inner surface and a high temperature on the upper surface, respectively. $0 \leq \left(\frac{r-a}{d-a}\right) \leq\sim 0.9$ The temperature increase as λ_3/λ_1 decrease and $0.9 \sim\leq \left(\frac{r-a}{d-a}\right) \leq 1$ temperature increases as λ_3/λ_1 increases. The temperature rises in the area $0 \leq \left(\frac{r-a}{d-a}\right) \leq\sim 0.9$ as λ_3/λ_1 decreases and rises $0.9 \sim\leq \left(\frac{r-a}{d-a}\right) \leq 1$ as λ_3/λ_1 increases. Furthermore, its is shown clearly that temperature remain identical at the location of $\left(\frac{r-a}{d-a}\right) \approx 0.85$. So it is evident that at that location heat transfer remain independent of thermal conductivity ratio λ_3/λ_1.

Figs. 12 and 13 show the effect of inner and outer surface thickness on temperature distributions, plotted along the radial direction. Each curve in Figs. 12 and 13 illustrates that when $\left(\frac{r-a}{d-a}\right)$ grows, the temperature falls. It is also clear that, as anticipated, the non-dimensional temperature is non-linear in the FGM core and linear in isotropic coatings.

Figs. 14 and 15 show the non-dimensional temperature θ of the inner and outer surfaces vs the ambient temperature ratio θ_d for the FG sandwich structure with varied Biot numbers Bi_2 (Figs. 14a and 15a) and radiation-conduction parameters N_r (Figs. 14b and 15b). Each of the curves in Figs. 14 and 15 demonstrates that the dimensionless temperature of the inner and outer surfaces rises when the ratio of ambient temperature θ_d increases. Furthermore, Figs. 14 and 15 indicate that the top and bottom surface temperatures drop

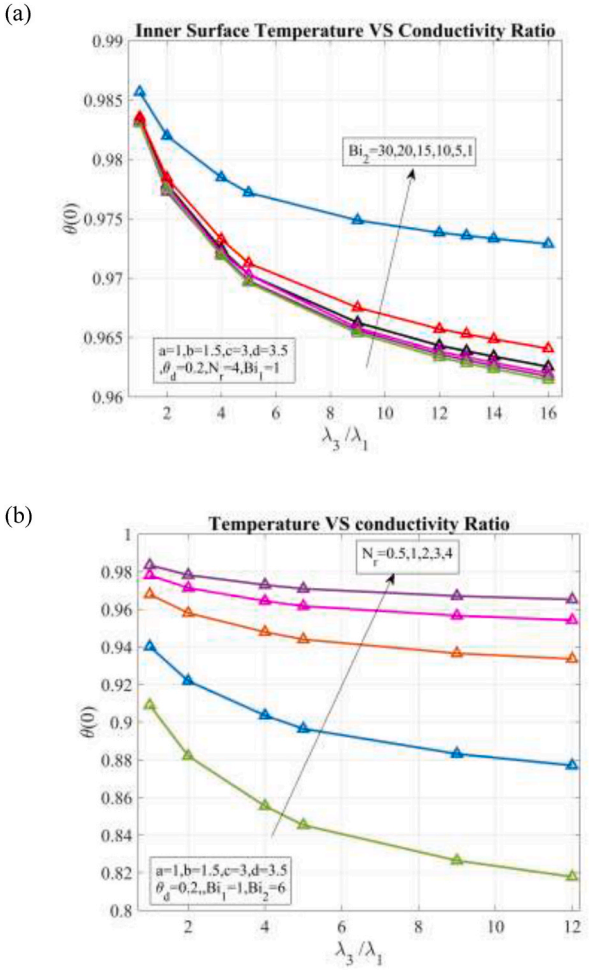

Fig. 18. Influence of the conductivity ratio $\left(\lambda_{3/\lambda_1}\right)$ on the inner surface temperature of FG sandwich structure with various values of (a) Biot number (Bi_2) and (b) radiation-conduction parameter (N_r).

with increasing Biot number Bi_2 and rise with increasing radiation-conduction parameters N_r. However, N_r has little effect on the temperature of the bottom surface.

Fig. 16 depicts the non-dimensional temperature of the inner coating vs the inner surface thickness for various Biot numbers Bi_2 and radiation-conduction parameters N_r. Moreover, Fig. 16 shows that for different thickness ratios, both temperature distributions appeared as dome shapes. Convection initially plays a major part in this increasing-decreasing pattern, but at a certain thickness, the addition of materials increases thermal resistance, which causes a fall in temperature. Furthermore, the critical radius of the insulation concept will be the best explanation in this regard. Again, the dome shape in Fig. 16b flattens as the Biot number decreases. The same explanation will be suited to this case.

Fig. 17 depicts the non-dimensional temperature of the outer coating vs the inner surface thickness for various Biot numbers Bi_2 and radiation-conduction parameters N_r. In this situation, the temperature at the outer surface continuously rises with the thickness ratio (Fig. 17a and b). Furthermore, the temperature rises as the Biot number falls, meaning that the least amount of heat will escape through the surface by convection (Fig. 17 a). Again, a higher radiation-conduction parameter results in a higher outer surface temperature (Fig. 17b).

Figs. 18 and 19 show, respectively, the temperature field of the inner and outer surfaces as functions of the conductivity ratio λ_{3/λ_1} for the FG composite structure with various Biot numbers Bi_2 (Figs. 18a and 19a) and radiation-conduction parameters N_r (Figs. 16b and 17b). Fig.s 18a, 19a show that temperature decreases as Biot number rises and a raise in the Biot number decreases for a particular value of conductivity ratio. This is because more heat loss by convection will result from larger outer surface Biot numbers, and reduced heat loss will result from smaller Biot numbers. Therefore, when the Biot number decreases, heat will accumulate and the temperature will rise. In addition, Figs. 18 and 19 also indicate that when the Biot number goes up, the temperature field of both the inner and outer surfaces goes down, and as the radiation-conduction parameter goes up, the temperature goes up. Moreover, In Fig. 20 (a–f), a FE visual demonstration has been provided for non-dimensional temperature distribution under various input parameters.

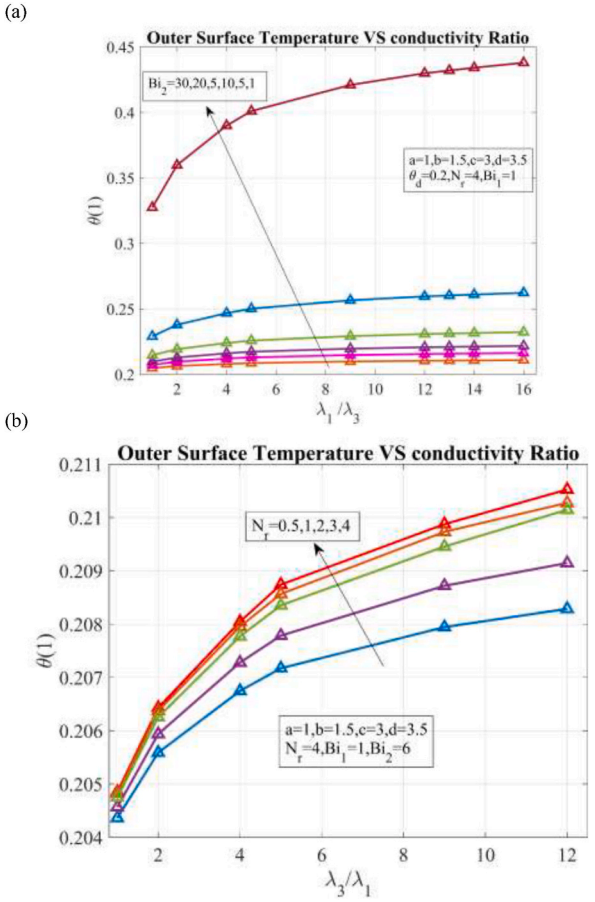

Fig. 19. Influence of the conductivity ratio $\left(\lambda_{3/\lambda_1}\right)$ on the inner surface temperature of FG sandwich with various values of (a) Biot number (Bi_2) and (b) radiation-conduction parameter (N_r).

4. Conclusion

1-D heat conduction consideration of radiation and convection in FGMs is crucial to the design and optimization of cylindrical structures for multifunctional areas pertinent to a variety of practical applications. In this study, the problem of heat conduction in inhomogeneous B.C.s is addressed analytically and numerically (FEA). Furthermore, For the first time, an exact and FEM solutions for steady-state heat transfer in FGM circular composite structures with convective-radiative boundary conditions was obtained. For both isotropic coatings and the FGM core, closed-form solutions, and numerical solutions were found and compared. It is also shown that there is good agreement between the analytical and numerical solutions. The advantage of the suggested method (exact and FEA) is that it may implement a variety of operating conditions, whether they are Dirichlet, Neumann, Robins, or nonlinear Neumann B.C.s. However, the following are the key findings of the present study:

i. The non-dimensional temperature fields θ for the FG circular sandwich structure is influenced differently by the inner and outer surface Biot numbers $(Bi_{i=1,2})$. The rise in the inner surface Biot number Bi_1 is accompanied by an increase in the dimensionless temperature. On the other hand, it decreases when the Biot number on the bottom surface Bi_2 grows up.
ii. Outer surface temperature $\theta(1)$ is more responsive to the temperature ratio θ_d parameter than the inner surface thickness ratio $r_{i=1/R_o}$.
iii. Since convection Bi_2 is so significant, the top surface temperature $\theta(0)$ may be lowered by boosting the conductivity ratio λ_{3/λ_1}, resulting in a drop in thermal resistance and enhanced heat transfer.
iv. The findings of this work are thought to be helpful for steady thermal analysis in FG circular sandwich structures, which will enhance thermal protection systems in nuclear reactors, aviation engineering, etc.

It is also concluded that the current study can be applied to the following future scopes:

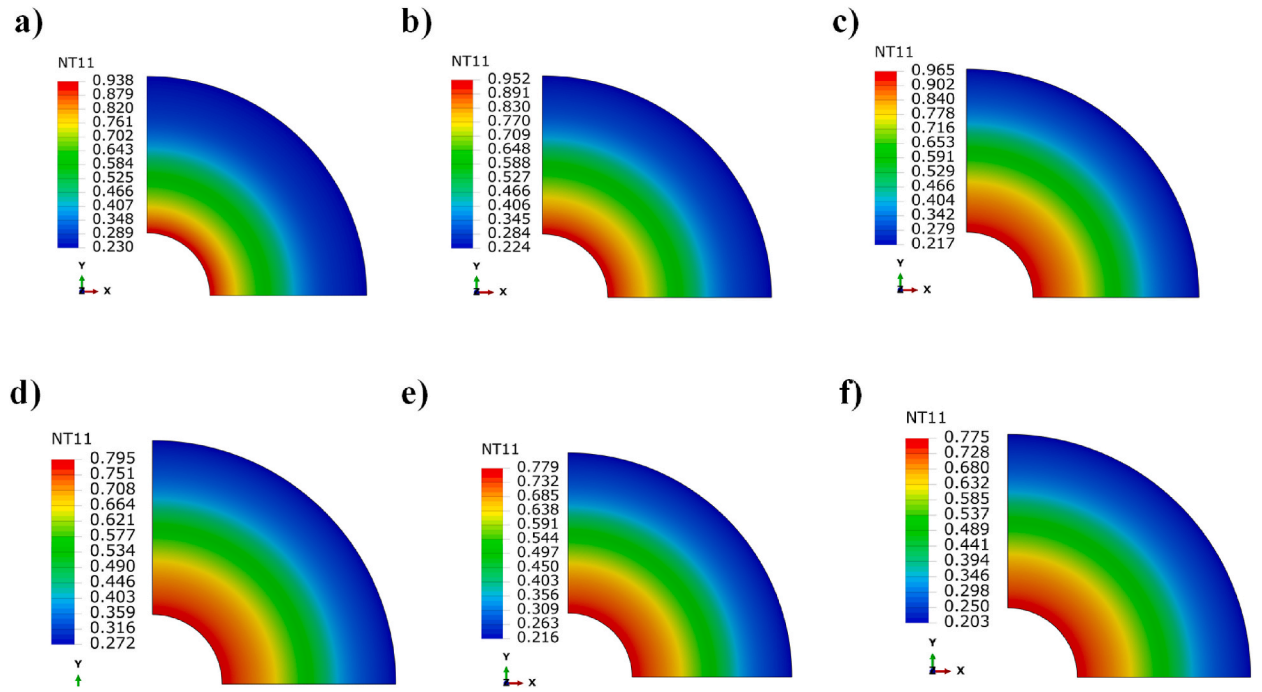

Fig. 20. Dimensionless temperature distribution are obtained through above mentioned FEA code for varying inhomogeneity (a) m = −3,(b) m = −4,(c) m = −5 and for varying Biot number (d) $Bi_2 = 1$,(e) $Bi_2 = 2$, and (f) $Bi_2 = 5$.

I. Material choice: Investigation of novel materials or materials in new combinations that can improve the performance of the FGM sandwich structure in a thermal environment.
II. Thermal Barrier Coatings: Improvement of the FGM sandwich structure's resilience to thermal stresses and temperature gradients. Creation of cutting-edge thermal barrier coatings.
III. Optimization and Design: Development of design techniques and optimization algorithms to improve the performance of FGM sandwich structures in thermal environments. This may entail employing computational tools, machine learning techniques, or genetic algorithms to determine optimal material distributions, layer thicknesses, or geometrical configurations.

Data availability

Data will be made available on request.

Additional information

No additional information is available for this paper.

Declaration of competing interest

The authors declare that they have no known competing financial interests or personal relationships that could have appeared to influence the work reported in this paper.

References

[1] L. Gray, et al., Green's functions and boundary integral analysis for exponentially graded materials: heat conduction, J. Appl. Mech. 70 (4) (2003) 543–549.
[2] Y. Ochiai, Two-dimensional steady heat conduction in functionally gradient materials by triple-reciprocity boundary element method, Eng. Anal. Bound. Elem. 28 (12) (2004) 1445–1453.
[3] L. Guo, N. Noda, Investigation methods for thermal shock crack problems of functionally graded materials–part I: analytical method, J. Therm. Stresses 37 (3) (2014) 292–324.
[4] Y. Zhang, L. Guo, N. Noda, Investigation methods for thermal shock crack problems of functionally graded materials–part II: combined analytical-numerical method, J. Therm. Stresses 37 (3) (2014) 325–339.
[5] L. Marin, Numerical solution of the Cauchy problem for steady-state heat transfer in two-dimensional functionally graded materials, Int. J. Solid Struct. 42 (15) (2005) 4338–4351.
[6] M.H. Babaei, Z. Chen, Transient hyperbolic heat conduction in a functionally graded hollow cylinder, J. Thermophys. Heat Tran. 24 (2) (2010) 325–330.
[7] A.M. Zenkour, Thermoelastic analysis of an annular sandwich disk with metal/ceramic faces and functionally graded core, J. Thermoplast. Compos. Mater. 22 (2) (2009) 163–181.

[8] R. Shirmohammadi, A. Moosaie, Non-Fourier heat conduction in a hollow sphere with periodic surface heat flux, Int. Commun. Heat Mass Tran. 36 (8) (2009) 827–833.
[9] M.H. Ghasemi, S. Hoseinzadeh, S. Memon, A dual-phase-lag (DPL) transient non-Fourier heat transfer analysis of functional graded cylindrical material under axial heat flux, Int. Commun. Heat Mass Tran. 131 (2022) 105858.
[10] M.H. Ghasemi, et al., Numerical analysis of non-fourier heat transfer in a solid cylinder with, dual-phase-lag 122 (1) (2020) 399–414.
[11] P. Malekzadeh, M. Golbahar Haghighi, Y. Heydarpour, Heat transfer analysis of functionally graded hollow cylinders subjected to an axisymmetric moving boundary heat flux, Numer. Heat Tran., Part A: Applications 61 (8) (2012) 614–632.
[12] P. Malekzadeh, R. Nejati, Non-fourier heat transfer analysis of functionally graded spherical shells under convection-radiation conditions. Journal of Oil, Gas and Petrochemical Technology 1 (1) (2014) 73–86.
[13] Abdelhak Mesbah, Z.B., Khaled Amara, Abdelouahed Tounsi, Abdelmoumen A. Bousahla, Fouad Bourada, Formulation and evaluation a finite element model for free vibration and buckling behaviours of functionally graded porous (FGP) beams. Structural Engineering and Mechanics, An Int 3 (2023) 291–309.
[14] P. Van Vinh, N. Van Chinh, A. Tounsi, Static bending and buckling analysis of bi-directional functionally graded porous plates using an improved first-order shear deformation theory and FEM, Eur. J. Mech. Solid. 96 (2022) 104743.
[15] T. Cuong-Le, et al., Nonlinear bending analysis of porous sigmoid FGM nanoplate via IGA and nonlocal strain gradient theory, Advances in nano research 12 (5) (2022) 441.
[16] Yogesh Kumar, A.G.a.A.T., Size-dependent vibration response of porous graded nanostructure with FEM and nonlocal continuum model, Advances in Nano Research (2021).
[17] Varun Katiyar, Ankit Gupta, A. Tounsi, *Microstructural/geometric imperfection sensitivity on the vibration response of geometrically discontinuous bi-directional functionally graded plates (2D FGPs) with partial supports by using FEM.* Steel and Composite Structures, Int. J. 45 (2022) 621–640.
[18] A. Garg, et al., Predicting elemental stiffness matrix of FG nanoplates using Gaussian Process Regression based surrogate model in framework of layerwise model, Eng. Anal. Bound. Elem. 143 (2022) 779–795.
[19] A.H.M. Abdeldjebbar Tounsi, Amina Attia, Anis Bousahla Abdelmoumen, Bourada Fouad, Tounsi Abdelouahed, Al-Osta Mohammed A., Free vibration investigation of functionally graded plates with temperaturedependent properties resting on a viscoelastic foundation, Structural Engineering and Mechanics, An Int 86 (1) (2023) 1.
[20] Ismail M. Mudhaffar, A.C., Abdelouahed Tounsi, Mohammed A. Al-Osta, Mesfer M. Al-Zahrani, Salah U. Al-Dulaijan *Impact of viscoelastic foundation on bending behavior of FG plate subjected to hygro-thermo-mechanical loads.* Structural Engineering and Mechanics, An Int ' l Journal 86 (2) (2023) 167–180.
[21] K. Bouafia, et al., Bending and free vibration characteristics of various compositions of FG plates on elastic foundation via quasi 3D HSDT model. Steel and Composite Structures, Int. J. 41 (4) (2021) 487–503.
[22] M. Hadji, et al., Combined influence of porosity and elastic foundation parameters on the bending behavior of advanced sandwich structures, Steel Compos. Struct. 46 (1) (2023) 1.
[23] N. Tutuncu, B. Temel, A novel approach to stress analysis of pressurized FGM cylinders, disks and spheres, Compos. Struct. 91 (3) (2009) 385–390.
[24] A. Benslimane, S. Bouzidi, M. Methia, Displacements and stresses in pressurized thick-walled FGM cylinders: exact and numerical solutions, Int. J. Pres. Ves. Pip. 168 (2018) 219–224.
[25] Y. Chen, X. Lin, Elastic analysis for thick cylinders and spherical pressure vessels made of functionally graded materials, Comput. Mater. Sci. 44 (2) (2008) 581–587.
[26] M.Z. Nejad, et al., Elastic analysis of exponential FGM disks subjected to internal and external pressure, Cent. Eur. J. Eng. 3 (2013) 459–465.
[27] K. Karami, et al., Elastic analysis of heterogeneous thick-walled spherical pressure vessels with parabolic varying properties, Front. Mech. Eng. 7 (2012) 433–438.
[28] L. You, J. Zhang, X. You, Elastic analysis of internally pressurized thick-walled spherical pressure vessels of functionally graded materials, Int. J. Pres. Ves. Pip. 82 (5) (2005) 347–354.
[29] S.A. Atashipour, R. Sburlati, S.R. Atashipour, Elastic analysis of thick-walled pressurized spherical vessels coated with functionally graded materials, Meccanica 49 (2014) 2965–2978.
[30] Y. Bayat, M. Ghannad, H. Torabi, Analytical and numerical analysis for the FGM thick sphere under combined pressure and temperature loading, Arch. Appl. Mech. 82 (2012) 229–242.
[31] P. Das, et al., Analytical and numerical analysis of functionally graded (FGM) axisymmetric cylinders under thermo-mechanical loadings, Mater. Today Commun. 33 (2022) 104405.
[32] R. Benchallal, et al., Analytical solution for rotating cylindrical FGM vessel subjected to thermomechanical loadings, Mater. Today: Proc. 53 (2022) 24–30.
[33] K. Celebi, D. Yarimpabuç, I. Keles, A novel approach to thermal and mechanical stresses in a FGM cylinder with exponentially-varying properties, J. Theor. Appl. Mech. 55 (1) (2017) 343–351.
[34] H.A. Sollund, K. Vedeld, J. Hellesland, Efficient analytical solutions for heated and pressurized multi-layer cylinders, Ocean engineering 92 (2014) 285–295.
[35] C. Evci, M. Gülgeç, Functionally graded hollow cylinder under pressure and thermal loading: effect of material parameters on stress and temperature distributions, Int. J. Eng. Sci. 123 (2018) 92–108.
[36] M. Jabbari, S. Sohrabpour, M. Eslami, Mechanical and thermal stresses in a functionally graded hollow cylinder due to radially symmetric loads, Int. J. Pres. Ves. Pip. 79 (7) (2002) 493–497.
[37] T. Sadowski, M. Birsan, D. Pietras, Multilayered and FGM structural elements under mechanical and thermal loads. Part I: comparison of finite elements and analytical models, Arch. Civ. Mech. Eng. 15 (4) (2015) 1180–1192.
[38] K. Abrinia, et al., New analysis for the FGM thick cylinders under combined pressure and temperature loading, Am. J. Appl. Sci. 5 (7) (2008) 852–859.
[39] Z. Shao, G. Ma, Thermo-mechanical stresses in functionally graded circular hollow cylinder with linearly increasing boundary temperature, Compos. Struct. 83 (3) (2008) 259–265.
[40] D. Sharma, R. Kaur, Thermoelastic analysis of FGM hollow cylinder for variable parameters and temperature distributions using FEM, Nonlinear Eng. 9 (1) (2020) 256–264.
[41] M. Eslami, M. Babaei, R. Poultangari, Thermal and mechanical stresses in a functionally graded thick sphere, Int. J. Pres. Ves. Pip. 82 (7) (2005) 522–527.
[42] A. Eldeeb, Y. Shabana, A. Elsawaf, Investigation of the thermoelastoplastic behaviors of multilayer FGM cylinders, Compos. Struct. 276 (2021) 114523.
[43] M. Meshkini, et al., Asymmetric mechanical and thermal stresses in 2D-FGPPMs hollow cylinder, J. Therm. Stresses 40 (4) (2017) 448–469.
[44] M. Jabbari, S. Sohrabpour, M. Eslami, General solution for mechanical and thermal stresses in a functionally graded hollow cylinder due to nonaxisymmetric steady-state loads, J. Appl. Mech. 70 (1) (2003) 111–118.
[45] M. Abualnour, et al., Thermomechanical analysis of antisymmetric laminated reinforced composite plates using a new four variable trigonometric refined plate theory. Computers and Concrete, Int. J. 24 (6) (2019) 489–498.
[46] N. Djilali, et al., Large cylindrical deflection analysis of FG carbon nanotube-reinforced plates in thermal environment using a simple integral HSDT. Steel and Composite Structures, Int. J. 42 (6) (2022) 779–789.
[47] M. Bendaida, et al., Dynamic properties of nonlocal temperature-dependent FG nanobeams under various thermal environments, Transport Porous Media 142 (1–2) (2022) 187–208.
[48] Z. Mazarei, M.Z. Nejad, A. Hadi, Thermo-elasto-plastic analysis of thick-walled spherical pressure vessels made of functionally graded materials, International Journal of Applied Mechanics 8 (4) (2016) 1650054.
[49] M.Z. Nejad, N. Alamzadeh, A. Hadi, Thermoelastoplastic analysis of FGM rotating thick cylindrical pressure vessels in linear elastic-fully plastic condition, Compos. B Eng. 154 (2018) 410–422.
[50] M. Nematollahi, A. Dini, M. Hosseini, Thermo-magnetic analysis of thick-walled spherical pressure vessels made of functionally graded materials, Appl. Math. Mech. 40 (2019) 751–766.
[51] M. Arefi, I. Nahas, Nonlinear electro thermo elastic analysis of a thick spherical functionally graded piezoelectric shell, Compos. Struct. 118 (2014) 510–518.

[52] K. Draiche, et al., An integral shear and normal deformation theory for bending analysis of functionally graded sandwich curved beams, Arch. Appl. Mech. 91 (2021) 4669–4691.
[53] P.S. Reddy, P. Sreedevi, A.J. Chamkha, Magnetohydrodynamic (MHD) boundary layer heat and mass transfer characteristics of nanofluid over a vertical cone under convective boundary condition, Propulsion and Power Research 7 (4) (2018) 308–319.
[54] P. Sreedevi, et al., Heat and mass transfer flow over a vertical cone through nanofluid saturated porous medium under convective boundary condition suction/injection, Journal of Nanofluids 6 (3) (2017) 478–486.
[55] P.S. Reddy, P. Sreedevi, A.J. Chamkha, Heat and mass transfer flow of a nanofluid over an inclined plate under enhanced boundary conditions with magnetic field and thermal radiation, Heat Tran. Asian Res. 46 (7) (2017) 815–839.
[56] P. Sreedevi, P.S. Reddy, A.J. Chamkha, Magneto-hydrodynamics heat and mass transfer analysis of single and multi-wall carbon nanotubes over vertical cone with convective boundary condition, Int. J. Mech. Sci. 135 (2018) 646–655.
[57] P. Sudarsana Reddy, P. Sreedevi, Heat and mass transfer analysis of single walled carbon nanotubes-water and multi wall carbon nanotubes-water based maxwell nanofluid flow over stretchable rotating disks, Journal of Nanofluids 12 (4) (2023) 1151–1159.
[58] A.A. Delouei, et al., Two-dimensional analytical solution for temperature distribution in FG hollow spheres: general thermal boundary conditions, Int. Commun. Heat Mass Tran. 113 (2020) 104531.
[59] A.A. Delouei, et al., On 2D asymmetric heat conduction in functionally graded cylindrical segments: a general exact solution, Int. J. Heat Mass Tran. 143 (2019) 118515.
[60] A.A. Delouei, et al., A closed-form solution for axisymmetric conduction in a finite functionally graded cylinder, Int. Commun. Heat Mass Tran. 108 (2019) 104280.
[61] A.A. Delouei, et al., Asymmetric conduction in an infinite functionally graded cylinder: two-dimensional exact analytical solution under general boundary conditions, J. Heat Tran. 142 (4) (2020), 044505.
[62] M. Kayhani, M. Norouzi, A.A. Delouei, A general analytical solution for heat conduction in cylindrical multilayer composite laminates, Int. J. Therm. Sci. 52 (2012) 73–82.
[63] V. Manthena, G. Kedar, Transient thermal stress analysis of a functionally graded thick hollow cylinder with temperature-dependent material properties, J. Therm. Stresses 41 (5) (2018) 568–582.
[64] A. Amiri Delouei, M. Norouzi, Exact analytical solution for unsteady heat conduction in fiber-reinforced spherical composites under the general boundary conditions, J. Heat Tran. 137 (10) (2015).
[65] C.-C. Ma, S.-W. Chang, Analytical exact solutions of heat conduction problems for anisotropic multi-layered media, Int. J. Heat Mass Tran. 47 (8–9) (2004) 1643–1655.
[66] S. Kumar, S.P. Mahulikar, Selection of materials and design of multilayer lightweight passive thermal protection system, J. Therm. Sci. Eng. Appl. 8 (2) (2016).
[67] M. Torabi, K. Zhang, Heat transfer and thermodynamic performance of convective–radiative cooling double layer walls with temperature-dependent thermal conductivity and internal heat generation, Energy Convers. Manag. 89 (2015) 12–23.
[68] X. Wang, et al., Exact analytical solution for steady-state heat transfer in functionally graded sandwich slabs with convective-radiative boundary conditions, Compos. Struct. 192 (2018) 379–386.
[69] A.A. Bousahla, et al., On thermal stability of plates with functionally graded coefficient of thermal expansion. Structural Engineering and Mechanics, An Int'l Journal 60 (2) (2016) 313–335.
[70] J. Dryden, K. Jayaraman, Effect of inhomogeneity on the stress in pipes, J. Elasticity 83 (2006) 179–189.
[71] M. Abramowitz, I.A. Stegun, Handbook of Mathematical Functions with Formulas, Graphs, and Mathematical Tables vol. 55, US Government printing office, 1948.
[72] T.W. Hungerford, Algebra, Springer Science & Business Media 73 (2012).